MNRAS **000**, 000–000 (0000) Preprint 29 September 2018 Compiled using MNRAS LATEX style file v3.0

Near and Mid-infrared properties of known $z \geq 5$ Quasars

Nicholas P. Ross[1]⋆ and Nicholas J. G. Cross[1]
[1]*Institute for Astronomy, University of Edinburgh, Royal Observatory, Edinburgh, EH9 3HJ, United Kingdom*

29 September 2018

ABSTRACT
In this paper, we, for the first time since the discovery of $z \geq 5$ quasars, assemble all spectroscopically confirmed very high redshift quasars in one catalogue. In particular we present the near ($zZyYJHK_s$ and K) infrared and mid-infrared (WISE) properties of all 424 spectroscopically confirmed redshift $z \geq 5.00$ quasars. Using archival public WFCAM/UKIRT and VIRCAM/VISTA data we check for photometric variability in the near-infrared that might be expected from Super-Eddington accretion and find *blah*. We present a comprehensive series of colour-redshift and colour-colour plots and make inferences into the hot dust properties of the very high-redshift quasar population. Extrapolating the known quasar luminosity function we suggest that x% of the possibly detected $z \geq 5$ quasars in the current datasets have been discovered.

Key words: Astronomical data bases: surveys – Quasars: general – galaxies: evolution – galaxies: infrared.

1 INTRODUCTION

Very high redshift quasars (VHzQ; defined here to have redshifts $z \geq 5.00$) are excellent probes of the early Universe. This includes studies of the Epoch of Reionization for hydrogen (see e.g. Fan et al. 2006; Mortlock 2016, for reviews), the formation and build-up of supermassive black holes (e.g., Rees 1984; Wyithe & Loeb 2003; Volonteri 2010; Agarwal et al. 2016; Valiante et al. 2018; Latif et al. 2018) and early metal enrichment (see e.g., Simcoe et al. 2012; Chen et al. 2017; Bosman et al. 2017).

Super-Eddington (also called super-critical) accretion is a viable physical mechanism to explain the high luminosity and rapid growth of supermassive black holes in the early universe (e.g., Alexander & Natarajan 2014; Madau et al. 2014; Volonteri et al. 2015; Pezzulli et al. 2016; Lupi et al. 2016; Pezzulli et al. 2017; Takeo et al. 2018). Thus, one might well expect VHzQs to vary in luminosity as they potentially go through phases of Super-Eddington accretion and these signatures of photometric variablity should be looked for, especially when the e.g. near-infrared K-band is sampling rest-frame ≈3670, 3145, 2750Å at redshifts $z = 5, 6$ and 7, respectively.

Quasars are also known to be prodigious emitters of infrared emission, thought to be from the thermal emission of dust grains heated by continuum emission from the accretion disc (e.g., Richards et al. 2006; Leipski et al. 2014; Hill et al. 2014; Hickox et al. 2017). Observations in the mid-infrared, e.g. ∼3-30μm allow discrimination between AGN[1] and passive galaxies due to the 1.6μm "bump" entering the MIR at $z \approx 0.8 - 0.9$ (e.g., Wright et al. 1994; Sawicki 2002; Lacy et al. 2004; Stern et al. 2005; Richards et al. 2006; Timlin et al. 2016) as well as AGN and star-forming galaxies due to the presence of Polycyclic Aromatic Hydrocarbon (PAHs) at $\lambda > 3\mu$m (e.g., Yan et al. 2007; Tielens 2008).

Jiang et al. (2006) and Jiang et al. (2010) report on the discovery of a quasar without hot-dust emission in a sample of 21 $z \approx 6$ quasars. Such apparently hot-dust-free quasars have no counterparts at low redshift. Moreover, those authors demonstrate that the hot-dust abundance in the 21 quasars builds up in tandem with the growth of the central black hole. Thus understanding how dust first forms and appears in the central engine remains an open question.

WISE mapped the sky in 4 passbands, in bands centered at wavelengths of 3.4, 4.6, 12, and 23μm. In total the release all sky "ALLWISE" catalog, contains nearly 750 million detections at high-significance[2]. Assef et al. (2013), Stern et al. (2012). Blain et al. (2013) presented WISE mid-infrared (MIR) detections of 17 (55%) of the then known 31 quasars at $z > 6$. However, Blain et al. (2013) was compiled with the WISE 'All-Sky' data release, as opposed to the superior "AllWISE" catalogs. That sample only examined the

⋆ Corresponding Author: npross@roe.ac.uk

[1] Historically, "quasars" and "Active Galactic Nuclei (AGN)" have described different luminosity/classes of objects, but here we use these terms interchangeably (with a preference for quasar) in recognition of the fact that they both describe accreting supermassive black holes (e.g. Haardt et al. 2016).
[2] wise2.ipac.caltech.edu/docs/release/allwise/expsup/sec2_1.html

31 known $z > 6$ quasars; our sample has 148 objects with redshift $z \geq 6.00$.

Here we update Jiang et al. (2010) and Blain et al. (2013) (along with Table 8 of Bañados et al. 2016). Our motivations are numerous and include: *(i)* establishing the first complete catalogue of $z > 5.00$ quasars since the pioneering work from SDSS; *(ii)* analysing all the WFCAM and VISTA [NJC: homogeneous isn't the write term. The NIR data is very heterogeneous] near-infrared photometry for the quasars; *(iii)* making the first study of NIR variability of the VHzQ population and *(iv)* establishing the photometric properties for upcoming surveys and telescopes, e.g. the Large Synoptic Survey Telescope (LSST) [3], ESA *Euclid*[4] and the *James Webb Space Telescope* (JWST)[5]

This paper can be considered an update of Blain et al. (2013) and also an extension of parts of Bañados et al. (2016), with the latter study reporting WISE W1, W2, W3 and W4 magnitudes for the Panoramic Survey Telescope and Rapid Response System 1 (Pan-STARRS1, PS1; Kaiser et al. 2002, 2010), but with no further investigation into the reddest WISE waveband for the VHzQs. Bañados et al. (2016) reports and investigates the W1, W2 and W3 properties of quasars at $z > 5.6$. We chose redshift $z = 5.00$ as our lower redshift limit due to a combination of garnishing a large sample, adequately spanning physical properties (e.g. luminosity, age of the Universe) and to incorporate what knowledge we have gained over the last couple of decades since $z > 5$ quasars were discovered.

This paper is organized as follows. In Section 2, we present the assembled list of the 424 $z \geq 5.00$ VHzQs that we have compiled. We then give a high-level overview of the photometric surveys and datasets we use and present the photometry of the VHzQs. **In Section 3 we** In Section 4 we and we then note our Conclusions in Section 5.

We make the somewhat unconventional decision [NJC: Is this unconventional?] to present all our photometry and magnitudes on the AB zero-point system (Oke & Gunn 1983; Fukugita et al. 1996). This includes the near-infrared, as well as the mid-infrared magnitudes. Because of established conventions, we report SDSS [NJC: PanSTARRS/DES rather than SDSS?] *ugriz* magnitudes on the AB zero-point system (Oke & Gunn 1983; Fukugita et al. 1996), while the WISE W1 4 magnitudes are calibrated on the Vega system (Wright et al. 2010). For WISE bands, $m_{\rm AB} = m_{\rm Vega} + m$ where m = (2.699, 3.339, 5.174, 6.66) for W1, W2, W3 and W4, respectively (Cutri et al. 2011; Brown et al. 2014). WFCAM and VISTA (**?**) are also calibrated on a Vega system (WFCAM), or near Vega system (VISTA). Brown et al. (2014), in PASA, is the paper about Recalibrating the Wide-field Infrared Survey Explorer (WISE) W4 Filter. We make use of the Explanatory Supplement to the WISE All-Sky Data Release, as well as the WISE AllWISE Data Release Products online. We use a flat ΛCDM cosmology with $H0 = 67.7$ km s−1 Mpc1, $\Omega_{\rm M} = 0.307$, and $\Omega_\Lambda = 0.693$ (Planck Collaboration et al. 2016) in order to be consistent with Bañados et al. (2016).

[3] lsst.org
[4] sci.esa.int/euclid/
[5] jwst.nasa.gov; sci.esa.int/jwst; www.asc-csa.gc.ca/eng/satellites/jwst; jwst.stsci.edu

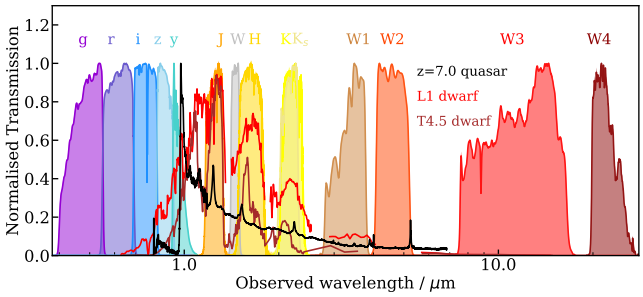

Figure 1. The spectral bands used by different survey telescopes and that are relevant here. The *grizy* filters are from the Pan-STARRS survey. The *JHK* are from UKIRT/WFCAM, while K_s is a VISTA/VIRCAM filter. The The narrow W-band centered at $\lambda \approx 14,500$Å is a CFHT/Wircam filter. [NJC: Do we use the W-band anywhere?] The WISE passbands W1-4 are also presented. The quasar spectrum is a composite based on Vanden Berk et al. (2001) and Bañados et al. (2016). The L and T dwarf spectra are from Cushing et al. (2006).

2 DATA

In Table 1 we present our dataset and we have assembled this in the following manner. First we compile the list of all known, spectroscopically confirmed quasars from the literature. Most of these objects are easily identified by their broad Lyα emission line, N v emission and characteristic shape blueward of 1215Å observed. As we shall see, some of the more recently discovered objects are close to the galaxy luminosity function characteristic luminosity M^*, and some have relatively weak or maybe even completely absorbed Lyα (e.g. Figures 7 and 10 in Bañados et al. 2016). We leave aside detailed investigation and discussion into espectral features and line strengths, and take as given the published spectra.

We then obtain optical, near-infrared and mid-infrared photometry for the spectral dataset. The optical data comes from the Panoramic Survey Telescope and Rapid Response System (Pan-STARRS) survey (Chambers et al. 2016) and the Dark Energy Camera (Flaugher et al. 2015), including the Dark Energy Survey (DES; Flaugher 2005) and the Dark Energy Camera Legacy Survey (Dey et al. 2018, DECaLS).

Recently, Hyper Suprime-Cam (HSC; Miyazaki et al. 2018) has embarked on the Subaru Strategic Program (SSP; Aihara et al. 2018b) delivering exquisite multi-band photometry data (Aihara et al. 2018a) the five broad bands *grizy*.

The near-infrared data comes from two primary sources. First, the Wide Field Camera (WFCAM; Casali et al. 2007) on the the United Kingdom Infra-Red Telescope (UKIRT) primarly, but not exclusively as part of the UKIRT Infrared Deep Sky Survey (UKIDSS; Lawrence et al. 2007). And second, data from the VIRCAM (VISTA InfraRed CAMera) on the VISTA (Visible and Infrared Survey Telescope for Astronomy; Emerson et al. 2006; Dalton et al. 2006).

We also obtain mid-infrared, $\lambda = 3 - 30\mu$m wavelength data from the the Wide-Field Infrared Survey Explorer (WISE; Wright et al. 2010; Cutri 2013) mission. WISE mapped the sky in 4 passbands, in bands centered at wavelengths of 3.4, 4.6, 12, and 23μm. In total the release all sky

"ALLWISE" catalog, contains nearly 750 million detections at high-significance[6].

Figure 1 displays the wavelength and normalised transmission of the filters in question.

[6] wise2.ipac.caltech.edu/docs/release/allwise/

na	desig	ra_hms	dec_dms	ra	dec	redshift	mag	M1450	ref
PSO	J000.3401+26.8358	00:01:21.63	+26:50:09.17	0.340113	+26.83588	5.75	19.52	-27.16	1/1/1
SDSS	J0002+2550	00:02:39.39	+25:50:34.80	0.664117	+25.84304	5.82	19.39	-27.31	5/22/1
SDSS	J0005-0006	00:05:52.34	-00:06:55.80	1.468083	-00.11549	5.85	20.98	-25.73	5/12/1
PSO	J002.1073-06.4345	00:08:25.77	-06:26:04.60	2.107390	-06.43456	5.93	20.41	-26.32	1;43/1/1
SDWISE	J0008+3616	00:08:51.43	+36:16:13.49	2.214292	+36.27041	5.17	19.12	-27.34	Wang2016
PSO	J002.3786+32.8702	00:09:30.89	+32:52:12.94	2.378702	+32.87026	6.1	21.13	-25.65	1/1/1
SDSS	J0017-1000	00:17:14.68	-10:00:55.4	4.311166	-10.01540	5.011	99.99	-99.99	DR7_W16
PSO	J004.3936+17.0862	00:17:34.47	+17:05:10.70	4.393614	+17.08631	5.8	20.69	-26.01	1/1/1
PSO	J004.8140-24.2991	00:19:15.38	-24:17:56.98	4.814080	-24.29920	5.68	19.43	-27.24	1/1/1
VDES	J0020-3653	00:20:31.46	-36:53:41.8	5.131124	-36.89495	6.9	99.99	-99.99	DES-VHS_inprep

Table 1. All 424 $z \geq 5.00$ quasars that have been spectroscopically confirmed as of 2018 June. The first ten objects are given here as guidance to the format of the data table. The full table can be found online.

na	desig	ra	dec	w1mag	w1err	w1snr	w2mag	w2err	w2snr	w3mag	w3err	w3snr	w4mag	w4err	w4snr
PSO	J000.3401+26.8358	0.34011348	26.83588138	16.373	0.066	16.5	15.266	0.107	10.2	12.594	0.492	2.2	8.756	-9.99	1.1
SDSS	J0002+2550	0.66411726	25.84304425	16.162	0.057	19.0	15.542	0.127	8.5	12.416	0.423	2.6	8.683	-9.99	1.2
SDSS	J0005-0006	1.4680833	-0.1154999	17.299	0.16	6.8	17.043	-9.99	0.2	12.445	-9.99	-1.1	9.008	-9.99	-0.3
PSO	J002.1073-06.4345	2.10739	-6.43456	16.809	0.107	10.1	15.684	0.141	7.7	11.892	-9.99	1.5	8.759	-9.99	0.2
SDWISE	J0008+3616	2.2142917	36.2704138	16.045	0.052	20.7	15.373	0.092	11.8	12.043	-9.99	1.8	8.786	-9.99	1.1
PSO	J002.3786+32.8702	2.37870183	32.87026179	-99.99	-9.99	-9.9	-99.99	-9.99	-9.9	-99.99	-9.99	-9.9	-9.99	-9.99	-9.9
SDSS	J0017-1000	4.3111666	-10.01539722	15.936	0.055	19.7	15.167	0.094	11.5	12.026	0.334	3.2	8.52	-9.99	1.2
PSO	J004.3936+17.0862	4.39361347	17.08630447	-99.99	-9.99	-9.9	-99.99	-9.99	-9.9	-99.99	-9.99	-9.9	-9.99	-9.99	-9.9
PSO	J004.8140-24.2991	4.81408	-24.29916	16.281	0.069	15.8	15.569	0.116	9.4	12.123	0.344	3.2	8.82	-9.99	0.5
VDES	J0020-3653	5.1311237	-36.8949476	16.844	0.094	11.6	16.354	0.204	5.3	12.679	-9.99	-0.1	8.342	-9.99	0.8

Table 2. The mid-infrared photometric properties from the WISE ALLWISE catalogue for the 424 very-high redshift quasars. The first ten objects are given here as guidance to the format of the data table. The full table can be found online. *This is the third table here; the SECOND table is this with the NIR data...*

na	desig	ra	dec	w1mag	w1err	w1snr	w2mag	w2err	w2snr	w3mag	w3err	w3snr	w4mag	w4err	w4snr
PSO	J000.3401+26.8358	0.34011348	26.83588138	16.373	0.066	16.5	15.266	0.107	10.2	12.594	0.492	2.2	8.756	-9.99	1.1
SDSS	J0002+2550	0.66411726	25.84304425	16.162	0.057	19.0	15.542	0.127	8.5	12.416	0.423	2.6	8.683	-9.99	1.2
SDSS	J0005-0006	1.4680833	-0.1154999	17.299	0.16	6.8	17.043	-9.99	0.2	12.445	-9.99	-1.1	9.008	-9.99	-0.3
PSO	J002.1073-06.4345	2.10739	-6.43456	16.809	0.107	10.1	15.684	0.141	7.7	11.892	-9.99	1.5	8.759	-9.99	0.2
SDWISE	J0008+3616	2.2142917	36.2704138	16.045	0.052	20.7	15.373	0.092	11.8	12.043	-9.99	1.8	8.786	-9.99	1.1
PSO	J002.3786+32.8702	2.37870183	32.87026179	-99.99	-9.99	-9.9	-99.99	-9.99	-9.9	-99.99	-9.99	-9.9	-9.99	-9.99	-9.9
SDSS	J0017-1000	4.3111666	-10.01539722	15.936	0.055	19.7	15.167	0.094	11.5	12.026	0.334	3.2	8.52	-9.99	1.2
PSO	J004.3936+17.0862	4.39361347	17.08630447	-99.99	-9.99	-9.9	-99.99	-9.99	-9.9	-99.99	-9.99	-9.9	-9.99	-9.99	-9.9
PSO	J004.8140-24.2991	4.81408	-24.29916	16.281	0.069	15.8	15.569	0.116	9.4	12.123	0.344	3.2	8.82	-9.99	0.5
VDES	J0020-3653	5.1311237	-36.8949476	16.844	0.094	11.6	16.354	0.204	5.3	12.679	-9.99	-0.1	8.342	-9.99	0.8

Table 3. The mid-infrared photometric properties from the WISE ALLWISE catalogue for the 424 very-high redshift quasars. The first ten objects are given here as guidance to the format of the data table. The full table can be found online. *This is the third table here; the SECOND table is this with the NIR data...*

2.1 Spectroscopy

We have obtained a list of 424 spectroscopically confirmed quasars with redshifts $z \geq 5.00$.

In Table 1 we give the discovery reference for the VHzQs noting that some objects were discovered independently and contemporaneously. The redshifts for the VHzQs generally come from the measurement of broad UV/optical emission lines. Where there are far infra-red emission lines e.g. C II 158 micron, we report these, but at the level of our current analysis broadline redshifts are sufficient.

Specifically, we use data from: Fan et al. (2000), Fan et al. (2001), Fan et al. (2003), Fan et al. (2004), Mahabal et al. (2005), Cool et al. (2006), Fan et al. (2006), Goto (2006), McGreer et al. (2006), Carilli et al. (2007), Kurk et al. (2007), Stern et al. (2007), Venemans et al. (2007), Willott et al. (2007), Jiang et al. (2008), Wang et al. (2008), Jiang et al. (2009), Kurk et al. (2009), Mortlock et al. (2009), Willott et al. (2009), Carilli et al. (2010), Wang et al. (2010), Willott et al. (2010), Willott et al. (2010), De Rosa et al. (2011), Mortlock et al. (2011), Wang et al. (2011), Zeimann et al. (2011), Morganson et al. (2012), Venemans et al. (2012), McGreer et al. (2013), Venemans et al. (2013), Wang et al. (2013), Willott et al. (2013), Bañados et al. (2014), Calura et al. (2014), Leipski et al. (2014), Bañados et al. (2015), Bañados et al. (2015), Becker et al. (2015), Carnall et al. (2015), Jiang et al. (2015), Kashikawa et al. (2015), Kim et al. (2015), Reed et al. (2015), Venemans et al. (2015b), Venemans et al. (2015a), Willott et al. (2015), Wu et al. (2015), Venemans et al. (2016), Wang et al. (2016), Matsuoka et al. (2016), Wang et al. (2016b), Mortlock et al. (2011), McGreer et al. (2013), Venemans et al. (2013), Venemans et al. (2013), Venemans et al. (2015b), Venemans et al. (2015a), Bañados et al. (2016), Matsuoka et al. (2016), Reed et al. (2017), Wang et al. (2017), Mazzucchelli et al. (2017), Ikeda et al. (2017), Tang et al. (2017), Koptelova et al. (2017), Bañados et al. (2018), Matsuoka et al. (2018a) and Matsuoka et al. (2018b).

Table 1 gives the salient details for the objects used in this study. We use all the $z \geq 5.00$ quasars that have been discovered and spectroscopically confirmed as of the time of writing (2018 June). We report near-infrared ($yYJHK$-bands) and mid-infrared (WISE W1/2/3/4) photometry and give our caculcated M_{1450}.

2.2 Optical Photometry

2.2.1 Pan-STARRS1 (PS1)

We query the Panoramic Survey Telescope and Rapid Response System (Pan-STARRS)[7] Data Release 1 (DR1) Catalog Archive Server Jobs System (CasJobs) service at mastweb.stsci.edu/ps1casjobs/. The PS1 survey observed the 30,000 deg^2 of sky north of declination -30 degrees in five filters $grizy$. Pan-STARRS1 (PS1) is the first part of Pan-STARRS to be completed and is the basis for the DR1. Chambers et al. (2016), Magnier et al. (2016c), Waters et al. (2016), Magnier et al. (2016a), Magnier et al. (2016b) and Flewelling et al. (2016) describe the instrument, survey, and data analyses. The principal science product of the PS1 survey is the catalog accessible through the CasJobs interface.

We query and return the mean PSF magnitudes from the $grizy$ filters (`MeanPSFMag`) which are in the AB system for our 424 VHzQ sample. Details of our SQL and links to the main tables are given in Appendix C.

[7] https://outerspace.stsci.edu/display/PANSTARRS

Survey	# VHzQs	Notes/Survey reference
ATLAS	4	Shanks et al. (2015)
CFHQS	20	Willott et al. (2007)
DELS	2	Dey et al. (2018)
ELAIS	1	Väisänen et al. (2000)
FIRST	1	Becker et al. (1995)
IMS	1	Kim et al. (2015)
MMT	12	McGreer et al. (2013)
NDWFS	1	Jannuzi & Dey (1999)
PSO	84	Kaiser et al. (2002, 2010)
RD	1	Mahabal et al. (2005)
SDSS	156	Stoughton et al. (2002)
SDUV	20	Yang et al. (2017)
SDWISE	27	Wang et al. (2016a)
SHELLQs	[a]63	Matsuoka et al. (2016)
ULAS	10	Lawrence et al. (2007)
VDES	11	Reed et al. (2017)
VIK	9	Edge et al. (2013)
VIMOS	1	Le Fèvre et al. (2003)

Table 4. The number of VHzQ from given surveys, with the key survey or telescope reference. [a]Includes 8 objects with a Hyper-SuprimeCam (HSC; Miyazaki et al. 2018) designation.

2.3 Near-infrared photometry

Due to their selection of being very faint/undetected in the observed-frame optical but bright in the observed frame near-infrared, VHzQs are generally detected in the near-infrared $yYJHK$-bands (≈0.98-2.38μm; e.g., Peth et al. 2011).

The near-infrared data in this paper comes from the Wide Field Astronomy Unit's (WFAU) Science Archives for UKIRT-WFCAM, the WFCAM Science Archive (WSA Hambly et al. 2008) and VISTA-VIRCAM, the VISTA Science Archive (VSA Cross et al. 2012). These archives were developed for the VISTA Data Flow System (VDFS Emerson et al. 2004).

In this paper we include all non-proprietary WFCAM data, which covers all public surveys and PI projects from Semester 05A to 1st January 2017 and all non-proprietary VISTA data, which covers all public surveys and PI projects from science verification (20091015) to 1st April 2016, to get as much coverage as possible. Hence, the NIR coverage is extremely heterogeneous.

The data was processed using a forced photometry, or matched-aperture photometry. A pipeline for this has been developed by WFAU, but has not yet been incorporated into the main VDFS pipeline. Full details of the matched-aperture pipeline (MAP) will appear in a forthcoming paper, Cross et al. 2018, in prep, and has also been discussed in Cross et al. (2013). We will give the pertinent points of the MAP and specific details of these data sets below.

The first step of the process was to ingest the catalogue of VHzQs into the WSA/VSA. These data are stored in the table `finalQsoCatalogue`. Next we set up new pro-

grammes WSERV1000, VSERV1000 in the WSA and VSA respectively. We assign all frames that potentially contain the high-z QSO based on WCS information in the WSA to WSERV1000, but adding a new line to the table `ProgrammeFrame` and same in VSA for VSERV1000. Assigning these frames to a separate programme allows us to process them together and put them into a single release.

2.3.1 Setup Matched Aperture Product

To create matched aperture products it is first necessary to define the product. We do this in two requirements tables, `RequiredMatchedApertureProduct` and `RequiredMapAverages` that tell the **ProgrammeBuilder** software which tables to create and what type of product is being created. These requirements tables also drive the pipeline.

`RequiredMatchedApertureProduct` contains the following attributes for the High-z QSO MAP product.

- mapID, Identifier of the MAP product, value=1
- archiveName, Main archive of product, value='VSA'/'WSA'
- programmeID, UID of programme, in this case a combined programme, value=10999
- extractor, Extractor used for forced photometry, value='CASU' (imcore_list)
- mapType, Type of MAP product (options 0 internal band-merged, 1 band-merged across surveys, 2 multi-epoch), value=2
- name, Name of MAP product, value='highzQsoMap'
- description, Description of MAP product, 'Variability via matched apertures for set of high-z QSOs'
- selection, Selection, e.g. File, pseudo-SQL, FITS image that is used to give input list, value='SELECTSTR qsoID,ra,dec FROMSTR finalQsoCatalogue'
- finalProductTable, Name of final product table, value='highzQsoMapVariability'
- addSurveyList, List of additional archive/surveys that data comes from, value='NONE'

`RequiredMatchedApertureProduct` gives all of the information such as the *programmeID* (identifying which data), the *mapType* (type of processing), the *extractor* to use, the input list *selection*, which in this case is the IDs and positions of the QSOs in `finalQsoCatalogue` which contains all the literature data and pre-derived parameters for the 424 QSOs.

`RequiredMapAverages` is used to setup the averaging of the MAP photometry from several images. We can average the epochs in multiple ways: over all the input images to a deep image, or similarly the input pawprint images to tile image in VISTA. Alternatively we can average over a fixed number of epochs or a fixed duration in time. Multiple setups can be defined in `RequiredMapAverages`, and the different averages selected using the defined *setupID*.

Add table?

2.3.2 Processing MAP data and Forced photometry

A set of apertures to do forced photometry with were created in `MapApertureIDshighzQsoMap`, based on the `RequiredMatchedApertureProduct` *selection* value, which in this case is to use the known positions of $z > 5$ QSOs. This may seem unnecessary layer since it is a one-to-one match with `finalQsoCatalogue`, but the layer is a general abstraction that allows multiple selections of data, including complex queries or input images.

CASU's `imcore_list` was run on each frame assigned to the programme with the input list equal to objects selected to be within ... of the multiframe centre. In this case, where there are 424 QSOs spread across the sky, there is typically 1 object per multiframe, but many have two and one frame, multiframeID=2614475 in the VSA (a J-band stack from a P90 PI programme), has 3 objects. The output of `imcore_list` is a multi-extension FITS binary table, with identical columns to the CASU FITS binary tables produced using the CASU `imcore`[8], the basis of all WFCAM and VISTA survey catalogue products and also familiar to many astronomers through the INTWFS, VST-ATLAS and VPHAS. Since forced photometry can be run in many ways on a particular image depending on the input catalogue, a single science frame is not necessarily linked to a single MAP catalogue, so the `MapFrameStatus` table links images (**multiframeID**) to catalogues (**catalogueID**). For matched aperture measurements, we process these binary tables using the same software, as the standard extracted catalogues, but implement a few different processes. We calculate both Luptitudes (Lupton et al. 1999), and calibrated fluxes, see Eqn 1.

$$F^{calib} = f \times 10^{-0.4*(ZP+VAB-8.90+corr)} \quad (1)$$

where f is the measured flux in ADU, ZP is the zeropoint of frame, VAB is the Vega-to-AB correction for the filter, and $corr$ are the various correction terms, e.g. distortion correction, scattered light correction, aperture correction, see (Hambly et al. 2008; Cross et al. 2012).

Once all data is processed, the data are ingested into `wserv1000MapRemeasurement` and `vserv1000MapRemeasurement` respectively. These tables are similar in structure to `lasDetection` described in (Hambly et al. 2008) or other UKIDSS or VISTA detection tables. One of the main differences is the primary key which is (**apertureID**,**catalogueID**) rather than (**multiframeID**,**extNum**,**seqNum**), reflecting the fact that these are forced photometry on a known set of apertures and a set of catalogues, rather than detections above a threshold in a set of detector extensions to image multiframes.

Quasars are known to vary (both photometrically and spectroscopically) and very high-z quasars under going super-Eddington accretion during a rapid BH growth phase are prime candidates for this variation. [NJC: This is better placed somewhere else. We first used it to justify averaging over 4 weeks, but then decided to average over many periods and select later.] Therefore, with repeat observations over many epochs available via the WSA, we have a choice to make for how we report the photometry. The remeasured photometry is averaged to improve signal-to-noise over all the averaging schemes setup in Table **??**. This allows us to

[8] http://casu.ast.cam.ac.uk/surveys-projects/vista/technical/catalogue-generation

programmeID	mapID	setupID	description	useDeeps	useHighProd	timeScale	nEpochs	overLaps
10999	1	0	Average over whole time	0	NONE	-1.000000	-99999999	1
10999	1	1	Average over a week	0	NONE	+7.000000	-99999999	1
10999	1	2	Average over a fortnight	0	NONE	+14.000000	-99999999	1
10999	1	3	Average over a month	0	NONE	+30.000000	-99999999	1
10999	1	4	Average over 10 epochs	0	NONE	-9.999995E008	10	1
10999	1	5	Average over 6 months	0	NONE	+183.000000	-99999999	1
10999	1	6	Average over 1 year	0	NONE	+365.000000	-99999999	1
10999	1	7	Average over 2 years	0	NONE	+730.000000	-99999999	1
10999	1	8	Average over 3 months	0	NONE	+91.000000	-99999999	1

Table 5.

get the best combination of signal-to-noise and number of epochs for different QSOs.

2.3.3 Averaging matched photometry

Unfortunately the photometry in a single epoch image often has low signal-to-noise. The advantage of matched aperture photometry on QSOs is that co-adding is relatively simple: if each epoch is taken in the same aperture (assuming the astrometry is correct) and the aperture photometry has been corrected to total: the standard aperture corrections work well for point sources then averaging the calibrated photometry should give as good as extracting from a deep stack. In fact it will almost certainly do better, since the images in some cases are taken from multiple projects with different pointings, and orientations and exposures, so stacking may not be optimal. In addition, corrections such as scattered light, pixel distortion and aperture corrections will be more complex, if not impossible to apply to deep-stacks but will be automatically applied in the averaging of forced photometry.

We average the aperture corrected calibrated fluxes (e.g. **aperJky3**), and then convert to magnitudes or luptitudes. Since we do not have a deep image for each set of averages, we cannot calculate non-aperture corrected values, so the photometry is only appropriate for point-sources.

$$\bar{F} = \frac{\sum_i^N (w_i\, F_i)}{\sum_i^N w_i} \qquad (2)$$

where F_i is the i^{th} epoch measurement of a parameter to be averaged such as the aperture corrected calibrated flux in a $1''$ aperture (**aperJky3**) and $\bar{F}$ is the weighted mean average of this parameter. The weight for each epoch $w_i = 1/(\sigma_F)^2$ if the epoch is included and $w_i = 0$ if an epoch is excluded for quality control purposes. We exclude inputs where the bitwise quality flag, **ppErrBits**¿256, and additionally, in the case of VISTA, we exclude data on detector 16 (**extNum=17**), where the quantum efficiency is variable. If all remeasurements are excluded, then one of the ones with the lowest **ppErrBits** is used. In this case the averages will be equal to the original measurement, and the reader may wonder why we bother to duplicate the data. It is important to do this to simplify queries for users who will then not have to set up complex queries to work out where the data is, and only around 2% of VISTA MAP measurements were excluded so the fraction of duplications is very low. The average data is stored in `wserv1000MapRemeasAver` for WFCAM and `vserv1000MapRemeasAver` for VISTA, which again are organised with a primary key of (**apertureID**,**catalogueID**). Some parameters that are averaged do not have an error σ_F, so in these cases we weight them using the **averageConf** parameter, which has a median of 100. In the case of WFCAM where this is not calculated, we set each epoch to have an **averageConf**= 100. The **sumWeights** parameter in the `MapRemeasAver` tables is the sum of all the **averageConf** values that went into the calculation and the `vserv1000MapAverageWeights` table gives the weights for each epoch, linked to each average for VSERV1000.

We calculate a set of averaged catalogues, for each pointing and filter, based on the requirements in `RequiredMapAverages`, in these cases over time spans of 7, 14, 30, 91, 183 days, 365 days, 730 days, over 10 epochs and over all epochs, see Tab. **??**. The averaging process starts at the first epoch and works on. Possible future refinements could first look for denser groupings that satisfied the criteria so that these were not split into two groups. For this high-z QSO project we have averaged over overlaps, because in several cases data for one source comes from multiple original projects that have slightly different pointings.

Each averaged catalogue has a separate entry in `MapFrameStatus` and is linked to each original epoch remeasured catalogue through `MapProvenance`, which contains the averaged catalogue identifier **combiCatID**, the epoch catalogue identifier **catalogueID** and the averaging setup ID **avSetupID**.

We give our recipe and SQL query syntax in Appendix D.

The code to calculate variability statistics as described in Cross et al. (2009) has not yet been completed to run with the matched aperture pipeline, so these are not included. Variables were selected ...

2.3.4 Selection of NIR variables

To select potentially variable QSOs we first did a selection like Appendix D(??), selecting the photometry averaged over the whole time span to assess the overall signal-to-noise, total timespan and number of measurements. For each QSO in each filter measured by each instrument, our initial selection for potential variables was $N_{\rm meas} \geq 8$, $T_{\rm tot} =_{\rm max} mjd - \min mjd > 30.$ days, $F > 0$. Jky and SNR¿8, to give a signal-to-noise of $\sim\geq 3$ per epoch and at least five measurements. An estimate was made of the number of useful epochs, such that $N_{\rm epc} = \min(N_{\rm meas}, \frac{SNR}{sqrt3.}$.

This in turn was used to estimate a typical time-scale for averaging, $T_{\rm avg} = \frac{T_{\rm tot}}{N_{\rm meas}}$.

We select average photometry where $(T_{\rm avg}/2.) \leq$ `RequiredMapAverages.timeScale` $\leq (2.*T_{\rm avg})$, a setup that should give the best combination of more epochs to resolve the variation and signal-to-noise per epoch. For each setup which satisfies this criteria, we get the averaged photometry and check the statistics. We calculate the median, and the median-absolute-deviation (MAD), and calculate the ratio of the standard deviation to the typical error, $r = \frac{1.48MAD}{\overline{error}/\sqrt{(N_{\rm epochs})}}$. Likely variables have $rat \geq 3.$ and $N_{\rm epoch} \geq 4$. Using this selection, we found two potential variables, xx and yy, both of which show variability in VISTA, with timescales of xn and ym, respectively. [Put in results]

As stated before, 114 QSOs have both WFCAM and VISTA data, and so some variables with fewer measurements in each, may also be variables. We took all of the intially selected variables that had both WFCAM and VISTA data, and looked for potential timescales in either WFCAM or VISTA, and if there was at least one good timescale, appropriate timescales were applied to both WFCAM and VISTA photometry: i.e. if a timescale of 30 days was found for WFCAM and 90 days for VISTA then the combined light curve would be averaged over 30 days for WFCAM and 90 days for VISTA; if only a 90 day average timescale for VISTA was found, then both WFCAM and VISTA would be averaged by 90 days, and if multiple averaging timescales were found, all suitable combinations would be tested. The same analysis of median and MAD was applied to the combined light-curves to find any additional potential variables. 2 more potential variables were found.

2.4 MIR data

The MIR data for this study comes exclusively from the Wide-field Infrared Survey Explorer (WISE) mission. Since we are only concerned here with the very large area ($\gg 1000$ deg^2) surveys, we leave exploration of the VHzQ population in e.g. the large Spitzer areal surveys such as the Spitzer IRAC Equatorial Survey (SpIES; Timlin et al. 2016), the Spitzer-HETDEX Exploratory Large-area Survey (SHELA; Papovich et al. 2016) and the Spitzer-SPT Deep Field (SSDF; Ashby et al. 2013), to a future investigation. This will also include a detailed study of MIR spectra e.g. Lambrides et al. (2018).

We use data from the the beginning of the WISE mission (2010 January; Wright et al. 2010) through the fourth-year of NEOWISE-R operations (Mainzer et al. 2011, 2017 December;). More specifically, we use the data from the AllWISE program and catalogue, which combines data from the WISE cryogenic and NEOWISE (Mainzer et al. 2011 ApJ, 731, 53) post-cryogenic survey phases. For the our variability investigations, we supplement the ALLWISE data with data from the NEOWISE 2018 Data Release. NEOWISE 2018 makes available the 3.4 and 4.6 m (W1 and W2) single-exposure images and extracted source information that were acquired between 2016 December 13 and 2017 December 13 UTC, which was the fourth year of survey operations of the Near-Earth Object Wide-field Infrared Survey Explorer Reactivation Mission (NEOWISE; Mainzer et al. 2014, ApJ, 792, 30). The fourth year NEOWISE data products are concatenated with those from the first three years (originally released on March 26, 2015, March 23, 2016 and June 1, 2017) into a single archive.

The WISE scan pattern leads to coverage of the full-sky approximately once every six months (a"sky pass"), but the satellite was placed in hibernation in 2011 February and then reactivated in 2013 October. Hence, our light curves have a cadence of 6 months with a 32 month sampling gap.

Selection	number detected (%)
Any band ($YJHK/K_s$	394 ( )
Y-band	( )
J-band	( )
H-band	( )
K or Ks-band	( )

Table 6. Detection rate of VHzQs in the near-infrared.

3 RESULTS

Having collated the sample of 424 VHzQs, and obtained their optical, near- and mid-infrared photometry we report here the various photometric properites of the quasars.

First, we will concentrate on detection rate in the infrared, go on to report on the color-redshift and color-color properties of our sample and then report on how the current sample populates the luminosity-redshift Lz-plane.

3.1 Detection Rates in the NIR

Table 6 gives the detection rates for the VHzQs in the NIR $YJHK/K_s$-bands. The first thing to note is that the coverage of the NIR surveys for example from the UKIDSS LAS and VISTA VHS, does not overlap the full area for where the VHzQs are detected.

3.1.1 Comparing WFCAM and VISTA

There are 114 overlapping QSOs between WFCAM and VISTA. Using the `VegaToAB` value[9] to put these objects on the same AB system, and for each object compared the two measurements. First, the calculated weighted average (calibrated flux) in each filter of both and calculated the ratio and difference between each measurement and the average. Then for each filter we calculated the weighted average of the differences (in mag) for each instrument to see if there were significant offsets. The results are given in Table 7. The only filter with a significant offset is the Y-band. All of the VISTA averages are negative and all of the WFCAM ones are positive. The Ks versus K band may be slightly dodgy, given the different shapes of the filters.

3.2 Detection Rates in the MIR

Unlike the NIR coverage, the WISE satellite and mission performed an all-sky survey, so the location of evey VHzQ in our dataset is covered. However, the depth of the WISE

[9] What is this exactly??

abs(VIRCAM - WFCAM)	millimags	no. of objects
Z	19.3	2
Y	66.2	48
J	3.2	105
H	19.3	89
K_s/K	12.7	93

Table 7. Comparing the magnitudes in different WFCAM/UKIRT and VIRCAM/VISTA near-infrared bands.

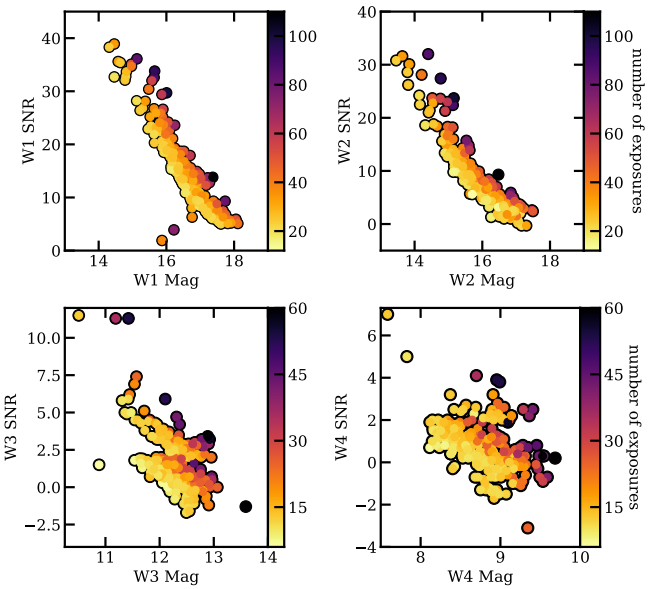

Figure 2. WISE W1/2/3/4 magnitude against signal-to-noise, colour coded by w$x$cov the mean coverage depth, in each corresponding band.

ALLWISE survey depends heavily on sky location, with locations near the Ecliptic Poles having the highest number of exposures.

Before reporting on the detection rates, we investigate this effect. Figure 3 shows the WISE magnitude versus signal-to-noise, colour coded by `wxcov` the mean coverage depth, in each corresponding band. In the two shorter bands W1/2 we see the clear and expected trend for brighter objects to have larger SNR, and also for the higher signal to noise for objects with more exposures at a given magnitude. The behaviour for the W3/4 bands is different, with two populations clearly evident in W3 and although a bit more mixed, also in W4. With the suggested split at SNR> 2, and no obvious R.A./Declination dependence seen, this behaviour is explained by the fact that there are non-detectiopns in W3/4 for objects (with high W1/2 SNR) that are reported in the ALLWISE catalogue.

For the 278 VHzQ with coverage detections, the mean number of exposures for the W1/2 bands is 32.0 and 31.5, respectively, with a minimum number of exposures 17 and 12, and the maximum number or exposures being 114 (for both bands). For the W3/4 filters, the corresponding mean, minimum and maximum exposure are 17.4 and 17.5, 5.8 and 6.8 and 69 (for both bands). These values are direclty from the `wxcov` enteries in the WISE ALLWISE catalogue.

Selection	number detected (%)
W1 SNR $>$ 2.0	275 (64.9)
W2 SNR $>$ 2.0	255 (60.1)
W1 $\wedge$ W2 SNR $>$ 2.0	
W3 SNR $>$ 2.0	99 (23.3)
W4 SNR $>$ 2.0	29 (6.8)
Any W1/2/3/4 SNR $>$ 2.0	
W1/2 SNR $<$ 2.0 $\wedge$ W3 SNR $>$ 2.0	

Table 8. ATLAS Shanks et al. (2015);

Selection	number detected (% of full specrta)
From "Source", "Rejects",	245, 40 (67.2)
W1 SNR $>$ 2.0	279 (65.8)
W2 SNR $>$ 2.0	258 (60.8)
W1 $\wedge$ W2 SNR $>$ 2.0	253 (59.7)
W3 SNR $>$ 2.0	97 (22.9)
W4 SNR $>$ 2.0	33 (7.8)
W1/2 SNR $<$ 2.0 $\wedge$ W3 SNR $>$ 2.0	3 (0.7)

Table 9. Data from the AllWISE Source Catalog and AllWISE Reject Table, from the `NASA/IPAC Infrared Science Archive`

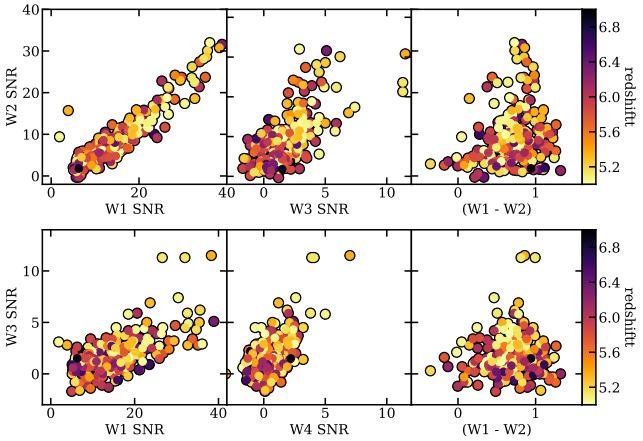

Figure 3. WISE signal-to-noise measures for the four bands, as well as for (W1-W2) colour. The points are colour coded by redshift.

Table 9 gives the detection rates for the VHzQs in the MIR WISE W1-4 bands.

Blain et al. (2013)

Recently, Assef et al. (2018) released two large catalogues of AGN candidates identified across 30,000 deg^2 of extragalactic sky from the WISE AllWISE Data Release. The "R90" catalogue, is contains 4.5M AGN candidates at 90% reliability (and ≈150 AGN candidates per deg^2) while the "C75" catalog consists of 20.9M AGN candidates at 75% completeness (and (≈700 AGN candidates per deg^2). Cross-matching out catalogue of 424 VHzQs with these catalogues, produces 42 matches with the R90 sample and 98 matches with the C75 sample. Both catalogues unsurprisingly match to the ultraluminous quasar SDSS J0100+2802 (Wu et al. 2015) while the C75, but not the R90 catalogue mathes to ULAS J1120+0641 (Mortlock et al. 2011). Neither catalogue matches J1342+0928 (Bañados et al. 2018).

Very High-z Quasars Detected in WISE W3 and W4.

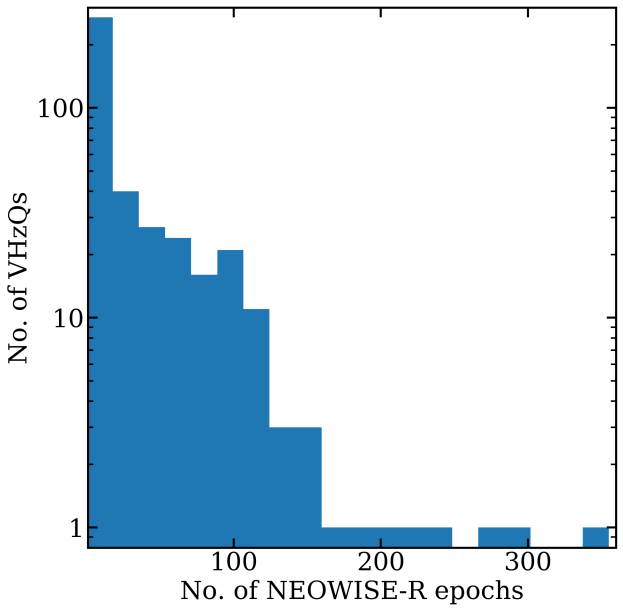

Figure 4. Histogram showing the number of NEOWISE-R epochs and detections there are for each VHzQ.

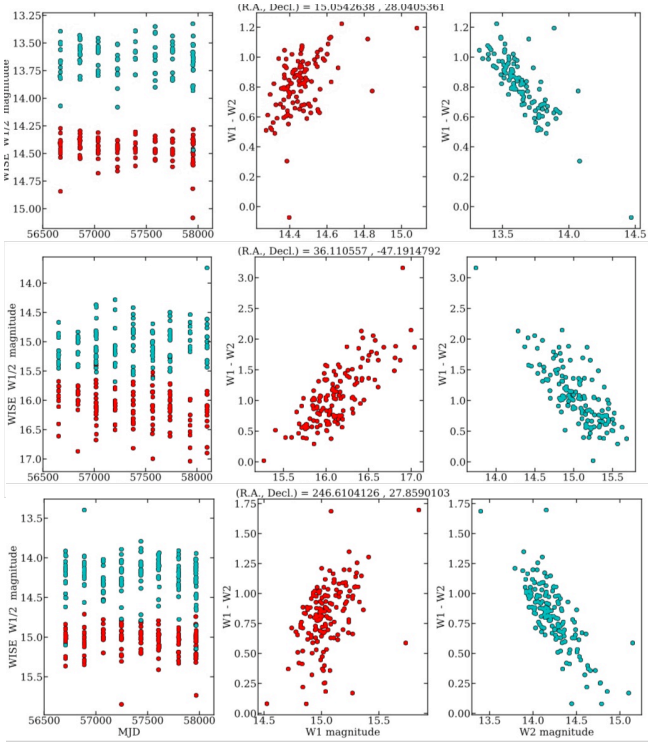

Figure 5. Here we show the MIR NEOWISE-R for J0100+2802 (Wu et al. 2015), J0224-4711 and J1626+2751. Red points are the W1 band; cyan points the W2 band.

3.3 Variability

VHzQs, if accreting at, or above the Eddington Limit, might well have have large values of changing mass accretion rate, $\ddot{m}_{\rm accr}$. A consequence of this would be that these quasar exhibit signs of variability, most likely showing up in their UV/optical rest-frame spectra. We look for evidence of this variability signature in the NIR and MIR light-curves of the VHzQs. As a guide, C IV enters the Y-band at redshift z=5.32 and exits at z=5.99, and enters the J-band at redshift $z = 6.55$ and exits at z=7.57. Mg II enters the H-band at redshift $z = 4.33$ and exits at $z = 5.37$ and enters the K-band at redshift $z = 6.25$ and exits at 7.50.

Using the extended datasets described in Section 2.3 and **??**, we

Figure 4 gives the number of NEOWISE-R epochs and detections there are for each VHzQ, while Figure **??** presents three examples of the MIR lighcurves and associated colour changes. Here we show J0100+2802 (Wu et al. 2015), J0224-4711 and J1626+2751.

3.4 Colours

Currently, very high-redshift quasars are identified by their morphology, flux and colours in optical and infrared imaging data Fan (1999); **?** Quasars are generally selected to be point sources, but be outliers from the stellar locus in colour space. For VHzQs, the main technique is to look for objects with extreme optical-to-near-infrared colours The lack of proper motion can also help identified quasars (e.g. Lang et al. 2009).

Pellentesque vel elit neque, in interdum lacus. Quisque sodales, nunc et luctus convallis, nisl dui luctus dui, at congue urna velit a nisl. Ut sit amet sapien a risus dapibus sagittis. Cras sed ultricies erat. Donec id metus sed urna lacinia convallis vel sed enim. Proin nisi libero, ornare vel bibendum eu, sollicitudin sed leo. Cras tincidunt aliquet ultricies. Cras pretium velit leo, in malesuada enim. Duis sagittis ultricies interdum. Proin sit amet sem nec metus feugiat pharetra.

Figure 6 presents the optical colour-redshift trends for Late Type M/L/T dwarfs and the VHzQs.

Figure 6 presents the near-infrared colour-redshift trends for Late Type M/L/T dwarfs and the VHzQs.

3.5 L-z Plane

Having obtained an as-near-to-homogenous set of photometry as we can, we are now in a position to calculate the Absolute Magnitudes of the VHzQ sample and in particulare the absolute magnitude at rest-frame 1450Å' M_{1450}, which is a key physical quantity and goes directly towards the quasar luminosity function and thus the reionization of hydrogen calculation.

At $z = 5.00$, the rest-frame 1450Å emission is redshifted to 8700Å iobserved, i.e., in the z-band, while at

3.6 SEDs and Dust properties of the VHzQs

There are a range of IR SEDs e.g. Mullaney et al. (2013) etc. etc. etc. However, they are, for our purposes all roughly the same.

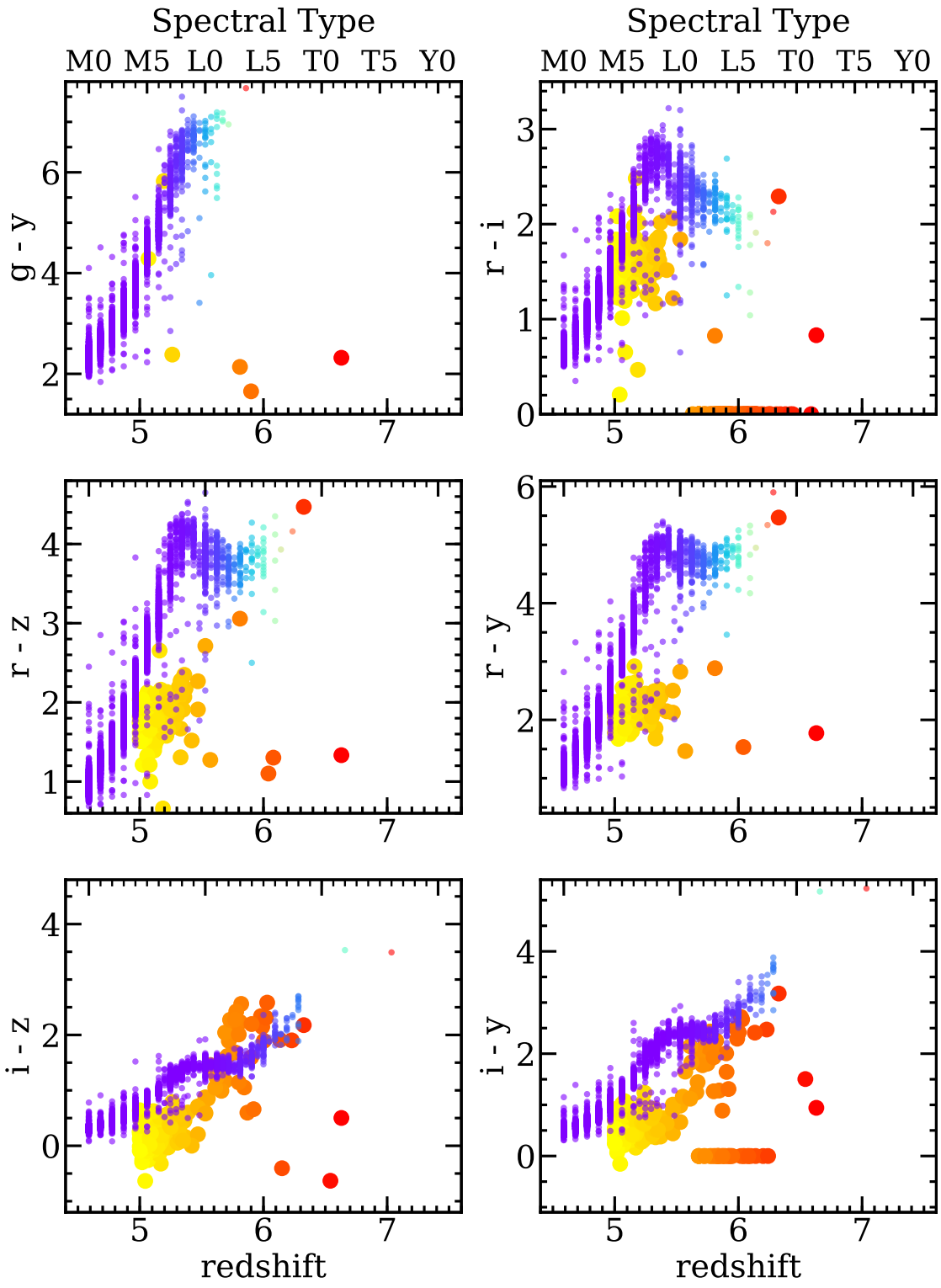

Figure 6. Optical colour vs. spectral type and redshift for Late Type M/L/T dwarfs and the VHzQs. The stars are M, L, and T dwarfs from the Best et al. (2018) PS1-detected catalog. *N.B. Trying to look as good as Fig. 5 from Best et al. (2018). How does one get bigger gaps between subplots??*

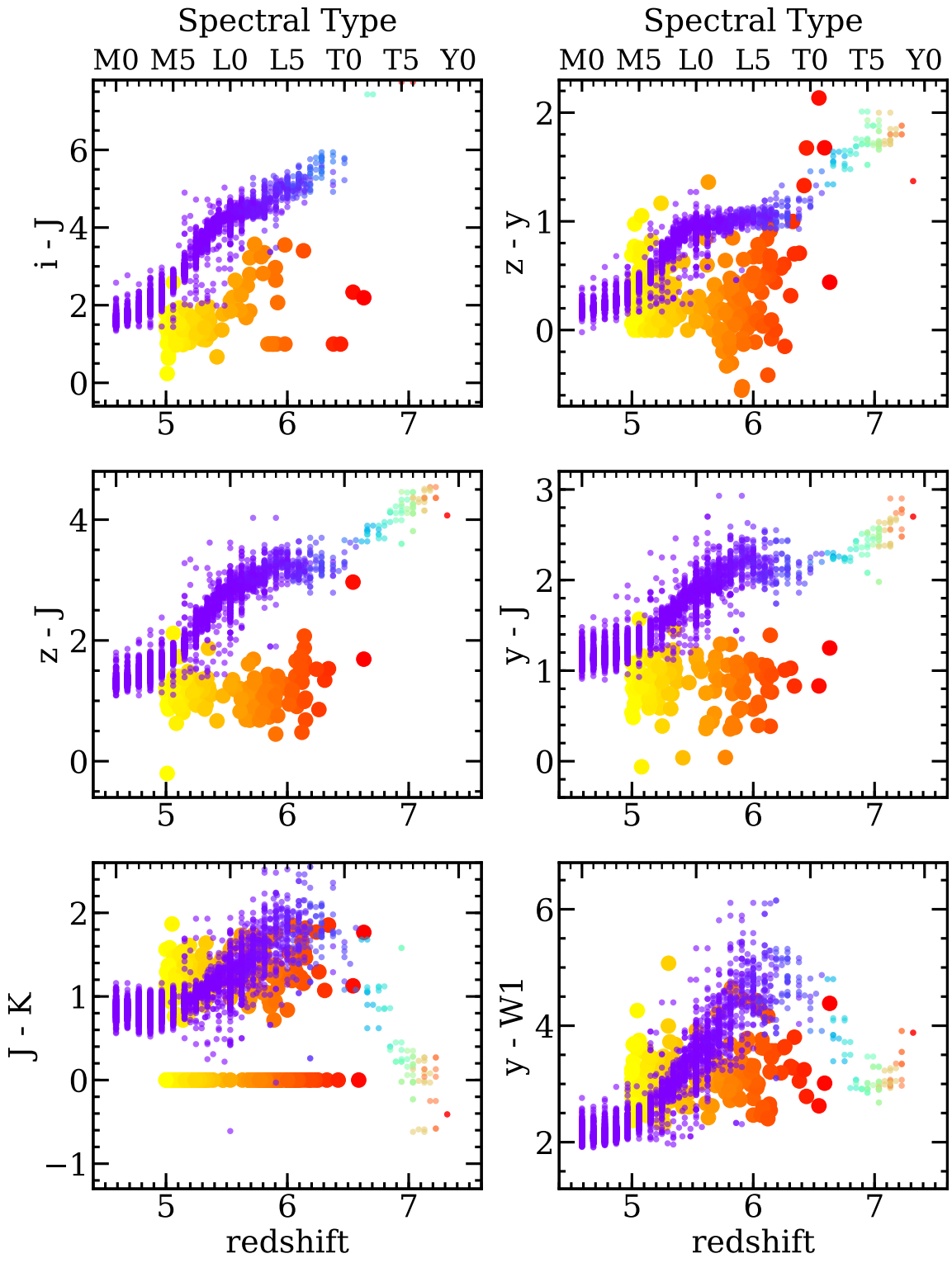

Figure 7. Infrared colour-spectral type and redshift plots for Late Type M/L/T dwarfs and the VHzQs. *NB* I'm really not sure how Best et al. actually get their stellar sequence so clean. There are two types of spectral classification, but restricting it to just SpT_optn or SpT_nir removes the blue or red end respectively. Hmmm....

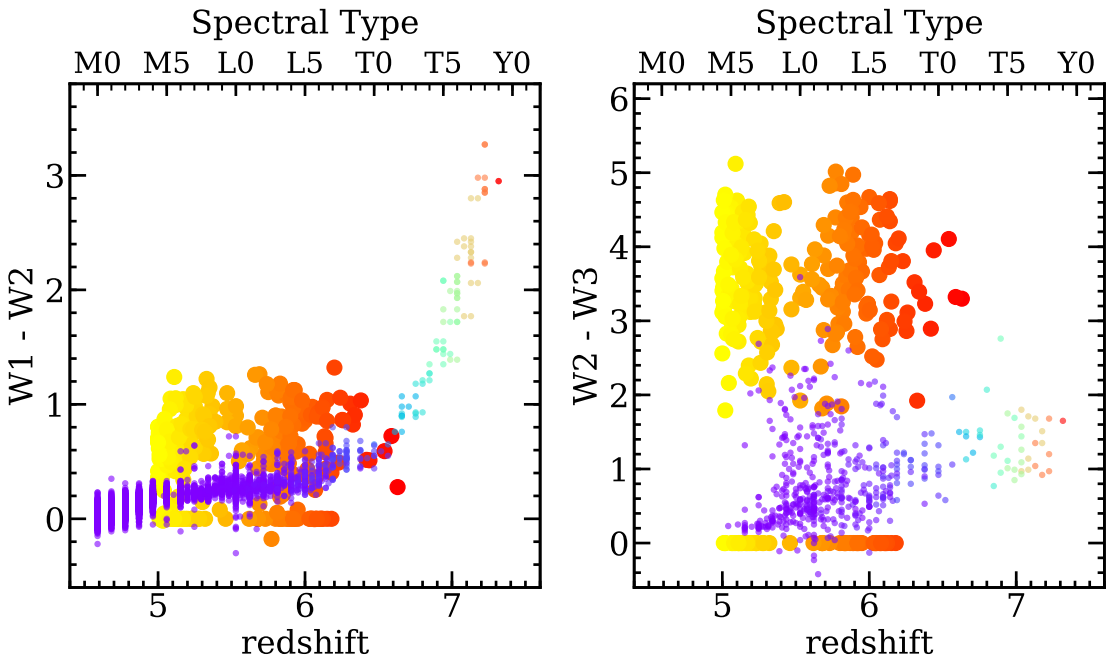

Figure 8. Infrared colour-spectral type and redshift plots for Late Type M/L/T dwarfs and the VHzQs.

4 DISCUSSION AND CONCLUSIONS

In this study, we have, for the first time, ompiled the list of all $z > 5$ spectroscopically confirmed quasars. We have assemble the NIR ($y/Y, J, H, K/K_s$) and MIR (WISE W1/2/3/4) photometry for these objects, given their detection rates and SEDs. We find that:

We can gain a good appreciation for what these missions will discover by collating the datasets we currently have.

- Lorem ipsum dolor sit amet, consectetur adipiscing elit. Aliquam porta sodales est, vel cursus risus porta non. Vivamus vel pretium velit. Sed fringilla suscipit felis, nec iaculis lacus convallis ac.
- Fusce pellentesque condimentum dolor, quis vehicula tortor hendrerit sed. Class aptent taciti sociosqu ad litora torquent per conubia nostra, per inceptos himenaeos. Etiam interdum tristique diam eu blandit. Donec in lacinia libero.
- Sed elit massa, eleifend non sodales a, commodo ut felis. Sed id pretium felis. Vestibulum et turpis vitae quam aliquam convallis. Sed id ligula eu nulla ultrices tempus. Phasellus mattis erat quis metus dignissim malesuada. Nulla tincidunt quam volutpat nibh facilisis euismod. Cras vel auctor neque. Nam quis diam risus.

Nunc lacus nibh, convallis ac lobortis ut, tempus ac lectus. Maecenas eu elit massa. Nulla vel lacus lorem. Proin et lobortis tortor. Phasellus ultrices nisl non enim porttitor dictum. Curabitur nec nunc ac nibh ornare elementum. Nunc ultrices hendrerit ultricies. Aliquam dapibus semper est et gravida. Etiam cursus, massa eget tempor elementum, lectus urna feugiat nisi, eget sagittis.

Author Contributions

N.P.R. initiated the project, compiled the list of $z > 5.00$ quasars, wrote most of the analysis code, developed the the plotting scripts, and developed and wrote the initial and subsequent drafts of the manuscript.

N.J.G.C. supplied the critical near-infrared expertise and database for which the bulk of the project relies. N.J.G.C. also contributed directly to the writing of the manuscript.

Availability of Data and computer analysis codes

All materials, data, code and analysis algorithms are fully available at: `https://github.com/d80b2t/VHzQ`

ACKNOWLEDGEMENTS

NPR acknowledges support from the STFC and the Ernest Rutherford Fellowship scheme.

We thank Mike Read at the ROE WFAU for help with the WFCAM Science Archiv (WSA), and also the VISTA Science Archive (VSA). We thank Bernie Shiao at STScI for help with the Pan-STARRS1 DR1 CasJobs interface.

This paper heavily used TOPCAT (v4.4) (Taylor 2005, 2011). This research made use of `Astropy`, a community-developed core Python package for Astronomy (Astropy Collaboration et al. 2013; The Astropy Collaboration et al. 2018).

The Pan-STARRS1 Surveys (PS1) and the PS1 public science archive have been made possible through contributions by the Institute for Astronomy, the University of Hawaii, the Pan-STARRS Project Office, the Max-Planck

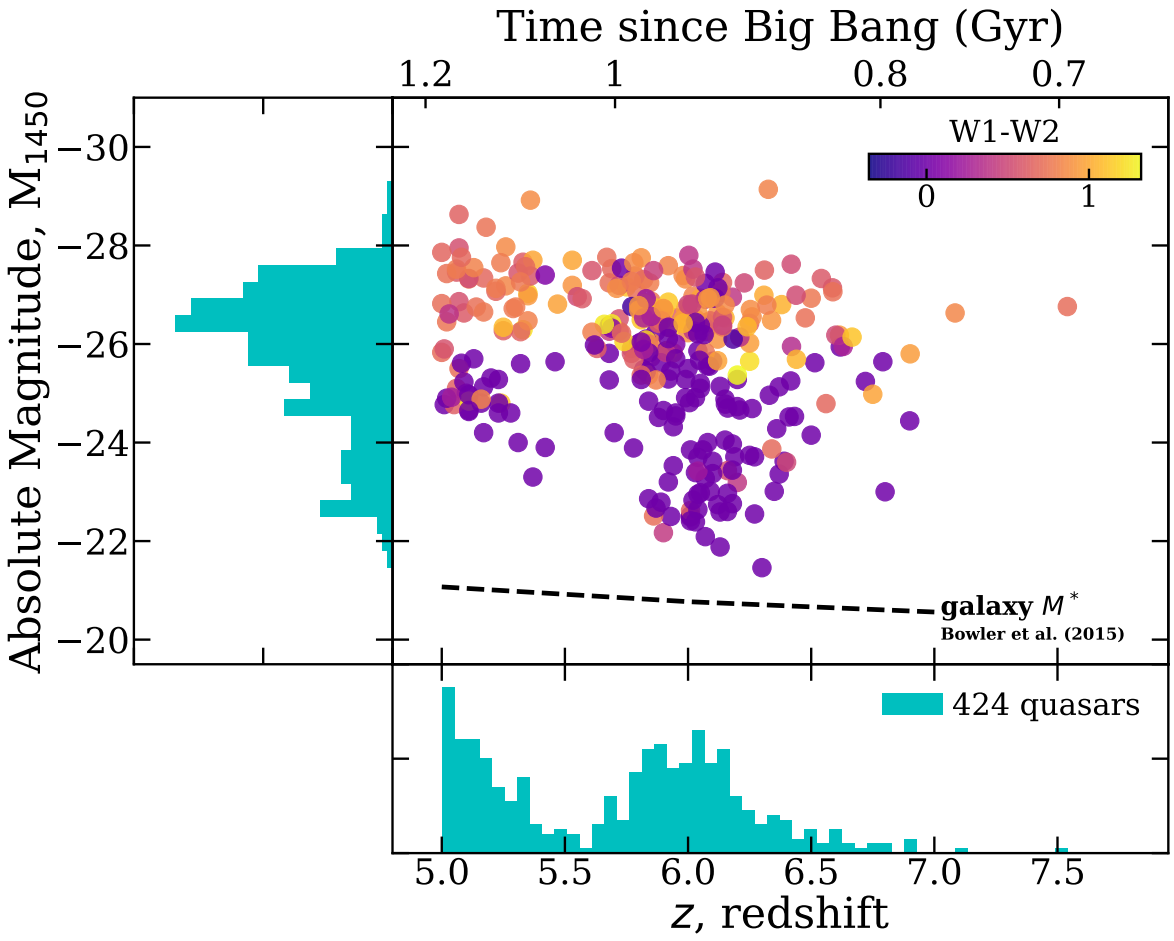

Figure 9. The spectral bands used by different survey telescopes and that are relevant here.

Society and its participating institutes, the Max Planck Institute for Astronomy, Heidelberg and the Max Planck Institute for Extraterrestrial Physics, Garching, The Johns Hopkins University, Durham University, the University of Edinburgh, the Queen's University Belfast, the Harvard-Smithsonian Center for Astrophysics, the Las Cumbres Observatory Global Telescope Network Incorporated, the National Central University of Taiwan, the Space Telescope Science Institute, the National Aeronautics and Space Administration under Grant No. NNX08AR22G issued through the Planetary Science Division of the NASA Science Mission Directorate, the National Science Foundation Grant No. AST-1238877, the University of Maryland, Eotvos Lorand University (ELTE), the Los Alamos National Laboratory, and the Gordon and Betty Moore Foundation.

This project used data obtained with the Dark Energy Camera (DECam) and the NOAO Data Lab, The Data Lab is operated by the National Optical Astronomy Observatory, the national center for ground-based nighttime astronomy in the United States operated by the Association of Universities for Research in Astronomy (AURA) under cooperative agreement with the National Science Foundation.

This publication makes use of data products from the Wide-field Infrared Survey Explorer, which is a joint project of the University of California, Los Angeles, and the Jet Propulsion Laboratory/California Institute of Technology, and NEOWISE, which is a project of the Jet Propulsion Laboratory/California Institute of Technology. WISE and NEOWISE are funded by the National Aeronautics and Space Administration.

CasJobs was originally developed by the Johns Hopkins University/ Sloan Digital Sky Survey (JHU/SDSS) team. With their permission, MAST used version 3.5.16 to construct CasJobs-based tools for GALEX, Kepler, the Hubble Source Catalog, and PanSTARRS.

This research has made use of the SVO Filter Profile Service (http://svo2.cab.inta-csic.es/theory/fps/) supported from the Spanish MINECO through grant AyA2014-55216 The SVO Filter Profile Service[10] describes the Spanish VO Filter Profile Service. The Filter

[10] Rodrigo, C., Solano, E., Bayo, A. http://ivoa.net/documents/Notes/SVOFPS/index.html

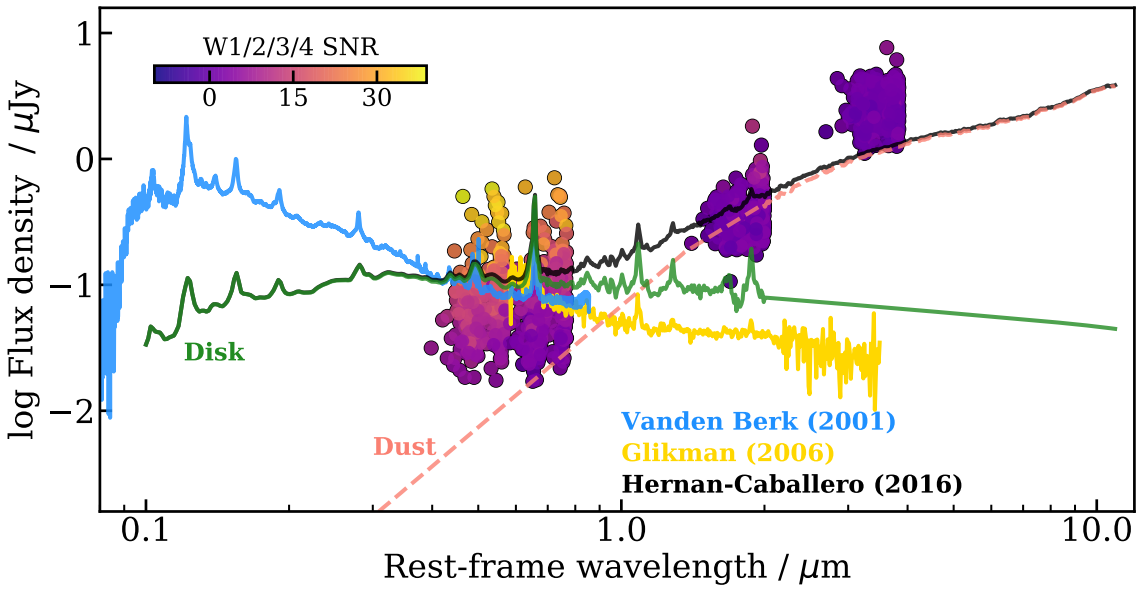

Figure 10. The rest-frame properties of the VHzQs.

Profile Service Access Protocol. Rodrigo, C., Solano, E. http://ivoa.net/documents/Notes/SVOFPSDAL/index.html

APPENDIX A: FILTER CURVES

FRom the SVO Filter Profile Service[11].

APPENDIX B: A. PHOTOMETRIC BANDS AND CONVERSIONS

Due to the differing normalizations between the SDSS and UKIDSS photometric systems, certain corrections are required. To present our data in the purest sense, all the NIR magnitudes from UKIDSS (originally AB magnitudes) were corrected to Vega magnitudes as suggested in Hewett et al. (2006).

Although ULAS magnitudes are reported in terms of Vega and SDSS magnitudes are reported in AB terms for the most part whenever an optical-NIR color was calculated both magnitudes were left in their default term.

https://www.gemini.edu/sciops/instruments/magnitudes-and-fluxes

APPENDIX C: PANSTARRS1 SQL QUERIES

The PS1 Casjobs SQL Server is located at mastweb.stsci.edu/ps1casjobs. The top level documentation is given here while the description of tables is given here. The main tables are the `objectThin` and `meanObject` tables.

[11] http://svo2.cab.inta-csic.es/svo/theory/fps/

Table B1. Adapted from Table 9 of Peth et al. (2011). CTIO/DECam, PanSTARRS/PS1, LSST Filter only values. All wavelengths in Å. From González-Fernández et al. (2018) $Z_{\rm AB} - Z_{\rm Vega} = 0.502$; $Y_{\rm AB} - Y_{\rm Vega} = 0.600$; $J_{\rm AB} - J_{\rm Vega} = 0.916$; $H_{\rm AB} - H_{\rm Vega} = 1.366$; $Ks_{\rm AB} - Ks_{\rm Vega} = 1.827$; and the CASU Vega to AB conversions v1.3:: Z,Y,J,H,Ks were: 0.524, 0.618, 0.937, 1.384, 1.839. So, Δ(vs. Gonzalez-Fernandez):: (11.2, 1.1, 5.4, 1.6, 0.1) millimags. Δ(vsCASU v1.3):: (-10.8, -16.9, -15.6, -16.4, -11.9) millimags.

Band	$\lambda_{\rm eff}$	$\lambda_{\rm min}$	$\lambda_{\rm max}$	W$_{\rm eff}$	AB - Vega	Transformations
$g_{\rm HSC}$	4633	3940	5546	1460	$g_{\rm HSC}$	$= g_{\rm AB} + 0.097$
$g_{\rm LSST}$	4730	3877	5665	1333	$g_{\rm LSST}$	$= g_{\rm AB} + 0.083$
$g_{\rm DECam}$	4734	3939	5528	1133	$g_{\rm DECam}$	$= g_{\rm AB} + 0.083$
$g_{\rm PS1}$	4776	3943	5593	1167	$g_{\rm PS1}$	$= g_{\rm AB} + 0.080$
$r_{\rm HSC}$	6104	5325	7071	1503	$r_{\rm HSC}$	$= r_{\rm AB} - 0.151$
$r_{\rm PS1}$	6130	5386	7036	1318	$r_{\rm PS1}$	$= r_{\rm AB} - 0.153$
$r_{\rm LSST}$	6139	5375	7055	1338	$r_{\rm LSST}$	$= r_{\rm AB} - 0.155$
$r_{\rm DECam}$	6345	5506	7238	1379	$r_{\rm DECam}$	$= r_{\rm AB} - 0.192$
$i_{\rm PS1}$	7485	6778	8304	1243	$i_{\rm PS1}$	$= i_{\rm AB} - 0.369$
$i_{\rm LSST}$	7487	6765	8325	1209	$i_{\rm LSST}$	$= i_{\rm AB} - 0.369$
$i_{\rm HSC}$	7633	6791	8658	1483	$i_{\rm PS1}$	$= i_{\rm AB} - 0.396$
$i_{\rm DECam}$	7750	6950	8646	1371	$i_{\rm DECam}$	$= i_{\rm AB} - 0.415$
$z_{\rm PS1}$	8658	8028	9346	966	$z_{\rm PS1}$	$= z_{\rm AB} - 0.508$
$z_{\rm LSST}$	8669	8035	9375	994	$z_{\rm LSST}$	$= z_{\rm AB} - 0.509$
$Z_{\rm VIRCAM}$	8762	8157	9400	978	$Z_{\rm VIRCAM}$	$= z_{\rm AB} - 0.513$
$Z_{\rm WFCAM}$	8802	8129	9457	926	$Z_{\rm WFCAM}$	$= z_{\rm AB} - 0.514$
$z_{\rm HSC}$	8915	8280	9498	793	$Z_{\rm HSC}$	$= z_{\rm AB} - 0.512$
$z_{\rm DECam}$	9216	8360	10166	1502	$z_{\rm DECam}$	$= z_{\rm AB} - 0.521$
$y_{\rm PS1}$	9603	9100	10838	615	$y_{\rm PS1}$	$= y_{\rm AB} - 0.541$
$y_{\rm LSST}$	9677	9089	10859	810	$y_{\rm LSST}$	$= y_{\rm AB} - 0.546$
$Y_{\rm DECam}$	9876	9355	10730	676	$Y_{\rm DECam}$	$= Y_{\rm AB} - 0.570$
$Y_{\rm HSC}$	9976	9000	10931	1386	$Y_{\rm HSC}$	$= Y_{\rm AB} - 0.580$
$Y_{\rm WFCAM}$	10305	9790	10810	1020	$Y_{\rm WFCAM}$	$= Y_{AB} - 0.617$
$Y_{\rm VIRCAM}$	10184	9427	10977	905	$Y_{\rm VISTA}$	$= Y_{AB} - 0.601$
$J_{\rm 2MASS}$	12350	10806	14068	1624	$J_{\rm 2MASS}$	$= J_{AB} - 0.894$
$J_{\rm VIRCAM}$	12464	11427	13759	1628	$J_{\rm VISTA}$	$= J_{AB} - 0.921$
$J_{\rm WFCAM}$	12483	11690	13280	1590	$J_{\rm WFCAM}$	$= J_{AB} - 0.919$
$W_{\rm Wircam}$	14514	13890	15166	1020	$W_{\rm Wircam}$	$= W_{AB} - 1.163$
$H_{\rm WFCAM}$	16313	14920	17840	2920	$H_{\rm WFCAM}$	$= H_{AB} - 1.379$
$H_{\rm VIRCAM}$	16310	14604	18422	2833	$H_{\rm VISTA}$	$= H_{AB} - 1.368$
$H_{\rm 2MASS}$	16620	14787	18231	2509	$H_{\rm 2MASS}$	$= H_{AB} - 1.374$
$Ks_{\rm VIRCAM}$	21337	19333	23674	3055	$Ks_{\rm VISTA}$	$= Ks_{AB} - 1.83$
$Ks_{\rm 2MASS}$	21590	19544	23552	2619	$Ks_{\rm 2MASS}$	$= Ks_{AB} - 1.84$
$K_{\rm WFCAM}$	22010	20290	23800	3510	$K_{\rm WFCAM}$	$= K_{AB} - 1.9$
WISE W1	33526	27541	38724	6626	W1	$= {\rm W1}_{\rm AB} - 2.699$
WISE W2	46028	39633	53414	10423	W2	$= {\rm W2}_{\rm AB} - 3.339$
WISE W3	115608	74430	172613	55056	W3	$= {\rm W3}_{\rm AB} - 5.174$
WISE W4	228172	195201	279107	41017	W4	$= {\rm W4}_{\rm AB} - 6.66$

```
SELECT s.ra, s.decl,
       o.objID, o.raMean, o.decMean,
       o.nDetections, o.ng, o.nr, o.ni, o.nz, o.ny,
       m.gMeanPSFMag, m.gMeanPSFMagErr,  m.gMeanPSFMagStd,
       m.rMeanPSFMag, m.rMeanPSFMagErr,  m.rMeanPSFMagStd,
       m.iMeanPSFMag, m.iMeanPSFMagErr,  m.iMeanPSFMagStd,
       m.zMeanPSFMag, m.zMeanPSFMagErr,  m.zMeanPSFMagStd,
       m.yMeanPSFMag, m.yMeanPSFMagErr,  m.yMeanPSFMagStd,
       s.jmag, s.jmag_error, s.hmag, s.hmag_error, s.kmag, s.kmag_error into mydb.MyTable_0 from M

```

```
11 cross apply fGetNearbyObjEq(s.ra,s.decl,2.0/60.0) nb
12 inner join ObjectThin o on o.objid=nb.objid and o.nDetections>1
13 inner join MeanObject m on o.objid=m.objid  and o.uniquePspsOBid=m.uniquePspsOBid
```

APPENDIX D: NEAR-INFRARED WFCAM SCIENCE ARCHIVE SQL QUERIES

Here we give the receipe and SQL that returned the near-infrared photometry for the VHzQs.

(i) http://wsa.roe.ac.uk/
(ii) Login
(iii) `username: WSERV1000; password: highzqso; community: nonSurvey`
(iv) Freeform SQL Query with WSERV1000v20180327

Then the following SQL will return the values in Table 1.

```
SELECT
qso.qsoName, qso.ra, qso.dec,
aver.apertureID, aver.aperJky3,
aver.aperJky3Err, aver.sumWeight,
aver.ppErrBits, m.mjdObs,
m.filterID, remeas.aperJky3,
remeas.aperJky3Err,
w.weight, remeas.ppErrBits,
m.project

FROM
highzQsoInput as qso,
MapApertureIDshighzQsoMap as ma,
wserv1000MapRemeasAver as aver,
wserv1000MapRemeasurement as remeas,
MapProvenance as v,
wserv1000MapAverageWeights as w,
MapFrameStatus as mfs,
Multiframe as m

WHERE
qso.qsoID=ma.objectID and
ma.apertureID=aver.apertureID and
aver.apertureID=remeas.apertureID and
aver.catalogueID=v.combicatID and
v.avSetupID=1 and
v.catalogueID=remeas.catalogueID and
w.combicatID=v.combicatID and
w.catalogueID=v.catalogueID and
w.apertureID=aver.apertureID and
mfs.catalogueID=remeas.catalogueID and
m.multiframeID=mfs.multiframeID and
mfs.programmeID=10999 and
mfs.mapID=1
order by v.combicatID, m.mjdObs
```

REFERENCES

Agarwal B., Smith B., Glover S., Natarajan P., Khochfar S., 2016, MNRAS, 459, 4209
Aihara H., et al., 2018a, PASJ, 70, S8
Aihara H., et al., 2018b, PASJ, 70, S4
Alexander T., Natarajan P., 2014, Science, 345, 1330
Ashby M. L. N., et al., 2013, ApJS, 209, 22
Assef R. J., et al., 2013, ApJ, 772, 26
Assef R. J., Stern D., Noirot G., Jun H. D., Cutri R. M., Eisenhardt P. R. M., 2018, ApJS, 234, 23
Astropy Collaboration et al., 2013, Astron. & Astrophys., 558, A33
Bañados E., Decarli R., Walter F., Venemans B. P., Farina E. P., Fan X., 2015, ApJ Lett., 805, L8
Bañados E., et al., 2014, AJ, 148, 14
Bañados E., et al., 2015, ApJ, 804, 118
Bañados E., et al., 2016, ApJS, 227, 11
Bañados E., et al., 2018, Nat, 553, 473
Becker G. D., Bolton J. S., Lidz A., 2015, PASA, 32, 45
Becker R. H., White R. L., Helfand D. J., 1995, ApJ, 450, 559
Best W. M. J., et al., 2018, ApJS, 234, 1
Blain A., et al., 2013, ArXiv e-prints
Bosman S. E. I., et al., 2017, MNRAS, 470, 1919
Brown M. J. I., Jarrett T. H., Cluver M. E., 2014, PASA, 31, 49
Calura F., Gilli R., Vignali C., Pozzi F., Pipino A., Matteucci F., 2014, MNRAS, 438, 2765
Carilli C. L., et al., 2007, ApJ Lett., 666, L9
Carilli C. L., et al., 2010, ApJ, 714, 834
Carnall A. C., Shanks T., Chehade B., Fumagalli M., Rauch M., Irwin M. J., Gonzalez-Solares E., Findlay J. R., Metcalfe N., 2015, MNRAS, 451, L16
Casali M., et al., 2007, Astron. & Astrophys., 467, 777
Chambers K. C., et al., 2016, arXiv:1612.05560v3
Chen S.-F. S., et al., 2017, ApJ, 850, 188
Cool R. J., et al., 2006, AJ, 132, 823
Cross N., Hambly N., Collins R., Sutorius E., Read M., Blake R., 2013, in Adamson A., Davies J., Robson I., eds, Thirty Years of Astronomical Discovery with UKIRT Vol. 37 of Astrophysics and Space Science Proceedings, Discovery of Variables in WFCAM and VISTA Data. p. 193
Cross N. J. G., Collins R. S., Hambly N. C., Blake R. P., Read M. A., Sutorius E. T. W., Mann R. G., Williams P. M., 2009, MNRAS, 399, 1730
Cross N. J. G., Collins R. S., Mann R. G., Read M. A., Sutorius E. T. W., Blake R. P., Holliman M., Hambly N. C., Emerson J. P., Lawrence A., Noddle K. T., 2012, Astron. & Astrophys., 548, A119
Cross N. J. G., et al., 2012, Astron. & Astrophys., 548, A119
Cushing M. C., et al., 2006, ApJ, 648, 614
Cutri R. M., et al., 2011, Technical report, Explanatory Supplement to the WISE Preliminary Data Release Products
Cutri R. M. o., 2013, Technical report, Explanatory Supplement to the AllWISE Data Release Products
Dalton G. B., et al., 2006, in Society of Photo-Optical Instrumentation Engineers (SPIE) Conference Series Vol. 6269 of Proc. SPIE, The VISTA infrared camera. p. 62690X
De Rosa G., Decarli R., Walter F., Fan X., Jiang L., Kurk J., Pasquali A., Rix H. W., 2011, ApJ, 739, 56
Dey A., et al., 2018, ArXiv e-prints
Edge A., Sutherland W., Kuijken K., Driver S., McMahon R., Eales S., Emerson J. P., 2013, The Messenger, 154, 32
Emerson J., McPherson A., Sutherland W., 2006, The Messenger, 126, 41
Emerson J. P., Irwin M. J., Lewis J., Hodgkin S., Evans D., Bunclark P., McMahon R., Hambly N. C., Mann R. G., Bond I., Sutorius E., Read M., Williams P., Lawrence A., Stewart M., 2004, in P. J. Quinn & A. Bridger ed., Society of Photo-Optical Instrumentation Engineers (SPIE) Conference Series Vol. 5493 of Society of Photo-Optical Instrumentation Engineers (SPIE) Conference Series, VISTA data flow system: overview. pp 401–410
Fan X., 1999, AJ, 117, 2528
Fan X., Carilli C. L., Keating B., 2006, ARA&A, 44, 415
Fan X., et al., 2000, AJ, 119, 1
Fan X., et al., 2004, AJ, 128, 515
Fan X., et al., 2006, AJ, 132, 117
Fan X., Narayanan V. K., Lupton R. H., Strauss M. A., Knapp G. R., Becker R. H., White R. L., Pentericci L., et al., 2001, AJ, 122, 2833
Fan X., Strauss M. A., Schneider D. P., Becker R. H., White R. L., Haiman Z., Gregg M., Pentericci L., et al., 2003, AJ, 125, 1649
Flaugher B., 2005, International Journal of Modern Physics A, 20, 3121
Flaugher B., et al., 2015, AJ, 150, 150
Flewelling H. A., et al., 2016, arXiv:1612.05243v2
Fukugita M., Ichikawa T., Gunn J. E., Doi M., Shimasaku K., Schneider D. P., 1996, AJ, 111, 1748
González-Fernández C., et al., 2018, MNRAS, 474, 5459
Goto T., 2006, MNRAS, 371, 769
Haardt F., Gorini V., Moschella U., Treves A., Colpi M., eds, 2016, Astrophysical Black Holes Vol. 905 of Lecture Notes in Physics, Berlin Springer Verlag
Hambly N. C., Collins R. S., Cross N. J. G., et al. 2008, MNRAS, 384, 637
Hambly N. C., et al., 2008, MNRAS, 384, 637
Hewett P. C., Warren S. J., Leggett S. K., Hodgkin S. T., 2006, MNRAS, 367, 454
Hickox R. C., Myers A. D., Greene J. E., Hainline K. N., Zakamska N. L., DiPompeo M. A., 2017, ApJ, 849, 53
Hill A. R., Gallagher S. C., Deo R. P., Peeters E., Richards G. T., 2014, MNRAS, 438, 2317
Ikeda H., Nagao T., Matsuoka K., Kawakatu N., Kajisawa M., Akiyama M., Miyaji T., Morokuma T., 2017, ApJ, 846, 57
Jannuzi B. T., Dey A., 1999, in Weymann R., et al. eds, ASP Conf. Ser. 191: Photometric Redshifts and the Detection of High Redshift Galaxies p. 111
Jiang L., et al., 2006, AJ, 132, 2127
Jiang L., et al., 2008, AJ, 135, 1057
Jiang L., et al., 2009, AJ, 138, 305
Jiang L., et al., 2010, Nat, 464, 380
Jiang L., McGreer I. D., Fan X., Bian F., Cai Z., Clément B., Wang R., Fan Z., 2015, AJ, 149, 188
Kaiser N., et al., 2002, in J. A. Tyson & S. Wolff ed., Society of Photo-Optical Instrumentation Engineers (SPIE) Vol. 4836, Pan-STARRS: A Large Synoptic Survey Telescope Array. pp 154–164
Kaiser N., et al., 2010, in Society of Photo-Optical Instrumentation Engineers (SPIE) Vol. 7733, The Pan-STARRS wide-field optical/NIR imaging survey. p. 0
Kashikawa N., Ishizaki Y., Willott C. J., Onoue M., Im M., Furusawa H., Toshikawa J., Ishikawa S., Niino Y., Shimasaku K., Ouchi M., Hibon P., 2015, ApJ, 798, 28
Kim Y., et al., 2015, ApJ Lett., 813, L35
Koptelova E., Hwang C.-Y., Yu P.-C., Chen W.-P., Guo J.-K., 2017, Scientific Reports, 7, 41617
Kurk J. D., et al., 2007, ApJ, 669, 32
Kurk J. D., Walter F., Fan X., Jiang L., Jester S., Rix H.-W., Riechers D. A., 2009, ApJ, 702, 833
Lacy M., et al., 2004, ApJS, 154, 166
Lambrides E. L., Petric A. O., Tchernyshyov K., Zakamska N. L., Watts D. J., 2018, ArXiv e-prints
Lang D., Hogg D. W., Jester S., Rix H., 2009, AJ, 137, 4400
Latif M. A., Volonteri M., Wise J. H., 2018, arXiv:1801.07685v1
Lawrence A., et al., 2007, MNRAS, 379, 1599

Le Fèvre O., et al., 2003, in Iye M., Moorwood A. F. M., eds, Instrument Design and Performance for Optical/Infrared Ground-based Telescopes Vol. 4841 of Proc. SPIE, Commissioning and performances of the VLT-VIMOS instrument. pp 1670–1681
Leipski C., et al., 2014, ApJ, 785, 154
Lupi A., Haardt F., Dotti M., Fiacconi D., Mayer L., Madau P., 2016, MNRAS, 456, 2993
Lupton R. H., Gunn J. E., Szalay A. S., 1999, AJ, 118, 1406
Madau P., Haardt F., Dotti M., 2014, ApJ Lett., 784, L38
Magnier E. A., et al., 2016a, arXiv:1612.05242v2
Magnier E. A., et al., 2016b, arXiv:1612.05244v2
Magnier E. A., et al., 2016c, arXiv:1612.05240v2
Mahabal A., Stern D., Bogosavljević M., Djorgovski S. G., Thompson D., 2005, ApJ Lett., 634, L9
Mainzer A., et al., 2011, ApJ, 731, 53
Matsuoka Y., et al., 2016, ApJ, 828, 26
Matsuoka Y., et al., 2018a, PASJ, 70, S35
Matsuoka Y., et al., 2018b, ApJS, 237, 5
Mazzucchelli C., et al., 2017, ApJ, 849, 91
McGreer I. D., Becker R. H., Helfand D. J., White R. L., 2006, ApJ, 652, 157
McGreer I. D., et al., 2013, ApJ, 768, 105
Miyazaki S., et al., 2018, PASJ, 70, S1
Morganson E., et al., 2012, AJ, 143, 142
Mortlock D., 2016, in Mesinger A., ed., Understanding the Epoch of Cosmic Reionization: Challenges and Progress Vol. 423 of Astrophysics and Space Science Library, Quasars as Probes of Cosmological Reionization. p. 187
Mortlock D. J., et al., 2009, Astron. & Astrophys., 505, 97
Mortlock D. J., et al., 2011, Nat, 474, 616
Mullaney J. R., Alexander D. M., Fine S., Goulding A. D., Harrison C. M., Hickox R. C., 2013, MNRAS, 433, 622
Oke J. B., Gunn J. E., 1983, ApJ, 266, 713
Papovich C., et al., 2016, ApJS, 224, 28
Peth M. A., Ross N. P., Schneider D. P., 2011, AJ, 141, 105
Pezzulli E., Valiante R., Schneider R., 2016, MNRAS, 458, 3047
Pezzulli E., Volonteri M., Schneider R., Valiante R., 2017, MNRAS, 471, 589
Reed S. L., et al., 2015, MNRAS, 454, 3952
Reed S. L., et al., 2017, MNRAS, 468, 4702
Rees M. J., 1984, ARA&A, 22, 471
Richards G. T., et al., 2006, ApJS, 166, 470
Sawicki M., 2002, AJ, 124, 3050
Shanks T., et al., 2015, MNRAS, 451, 4238
Simcoe R. A., Sullivan P. W., Cooksey K. L., Kao M. M., Matejek M. S., Burgasser A. J., 2012, Nat, 492, 79
Stern D., et al., 2005, ApJ, 631, 163
Stern D., et al., 2007, ApJ, 663, 677
Stern D., et al., 2012, ApJ, 753, 30
Stoughton C., et al., 2002, AJ, 123, 485
Takeo E., Inayoshi K., Ohsuga K., Takahashi H. R., Mineshige S., 2018, MNRAS, 476, 673
Tang J.-J., et al., 2017, MNRAS, 466, 4568
Taylor M., , 2011, TOPCAT: Tool for OPerations on Catalogues And Tables, Astrophysics Source Code Library
Taylor M. B., 2005, in Shopbell P., Britton M., Ebert R., eds, Astronomical Data Analysis Software and Systems XIV Vol. 347 of Astronomical Society of the Pacific Conference Series, TOPCAT & STIL: Starlink Table/VOTable Processing Software. p. 29
The Astropy Collaboration et al., 2018, ArXiv e-prints
Tielens A. G. G. M., 2008, ARA&A, 46, 289
Timlin J. D., Ross N. P., et al., 2016, ApJS, 225, 1
Väisänen P., Tollestrup E. V., Willner S. P., Cohen M., 2000, ApJ, 540, 593
Valiante R., Schneider R., Graziani L., Zappacosta L., 2018, MNRAS, 474, 3825
Vanden Berk D. E., et al., 2001, AJ, 122, 549
Venemans B. P., et al., 2012, ApJ Lett., 751, L25
Venemans B. P., et al., 2013, ApJ, 779, 24
Venemans B. P., et al., 2015a, MNRAS, 453, 2259
Venemans B. P., et al., 2015b, ApJ Lett., 801, L11
Venemans B. P., McMahon R. G., Warren S. J., Gonzalez-Solares E. A., Hewett P. C., Mortlock D. J., Dye S., Sharp R. G., 2007, MNRAS, 376, L76
Venemans B. P., Walter F., Zschaechner L., Decarli R., De Rosa G., Findlay J. R., McMahon R. G., Sutherland W. J., 2016, ApJ, 816, 37
Volonteri M., 2010, A&ARv, 18, 279
Volonteri M., Silk J., Dubus G., 2015, ApJ, 804, 148
Wang F., et al., 2016a, ApJ, 819, 24
Wang F., et al., 2017, ApJ, 839, 27
Wang F., Wu X.-B., Fan X., Yang J., Yi W., Bian F., McGreer I. D., Yang Q., Ai Y., Dong X., Zuo W., Jiang L., Green R., Wang S., Cai Z., Wang R., Yue M., 2016, ApJ, 819, 24
Wang R., et al., 2008, ApJ, 687, 848
Wang R., et al., 2010, ApJ, 714, 699
Wang R., et al., 2011, ApJ Lett., 739, L34
Wang R., et al., 2013, ApJ, 773, 44
Wang R., et al., 2016b, ApJ, 830, 53
Waters C. Z., et al., 2016, arXiv:1612.05245v4
Willott C. J., Albert L., Arzoumanian D., Bergeron J., Crampton D., Delorme P., Hutchings J. B., Omont A., Reylé C., Schade D., 2010, AJ, 140, 546
Willott C. J., Bergeron J., Omont A., 2015, ApJ, 801, 123
Willott C. J., et al., 2007, AJ, 134, 2435
Willott C. J., et al., 2009, AJ, 137, 3541
Willott C. J., et al., 2010, AJ, 139, 906
Willott C. J., Omont A., Bergeron J., 2013, ApJ, 770, 13
Wright E. L., Eisenhardt P. E., Fazio G. G., 1994, ArXiv Astrophysics e-prints
Wright E. L., et al., 2010, AJ, 140, 1868
Wu X.-B., et al., 2015, Nat, 518, 512
Wyithe J. S. B., Loeb A., 2003, ApJ, 586, 693
Yan L., Sajina A., Fadda D., Choi P., Armus L., Helou G., Teplitz H., Frayer D., Surace J., 2007, ApJ, 658, 778
Yang Q., et al., 2017, ArXiv e-prints
Zeimann G. R., White R. L., Becker R. H., Hodge J. A., Stanford S. A., Richards G. T., 2011, ApJ, 736, 57